Sameer S. Kulkarni,[1] Magali Joffraud,[1] Marie Boutant,[1] Joanna Ratajczak,[1,2] Arwen W. Gao,[3] Catherine Maclachlan,[2] Maria Isabel Hernandez-Alvarez,[4,5,6] Frédéric Raymond,[1] Sylviane Metairon,[1] Patrick Descombes,[1] Riekelt H. Houtkooper,[3] Antonio Zorzano,[4,5,6] and Carles Cantó[1,2]

Mfn1 Deficiency in the Liver Protects Against Diet-Induced Insulin Resistance and Enhances the Hypoglycemic Effect of Metformin

Diabetes 2016;65:3552–3560 | DOI: 10.2337/db15-1725

Mitochondrial function can be influenced by mitochondrial shape and connectivity with other cellular organelles through fusion and fission processes. Disturbances in mitochondrial architecture and mitochondrial fusion-related genes are observed in situations of type 2 diabetes and obesity, leading to a highly fissioned mitochondrial network. To directly test the effect of reduced mitochondrial fusion on hepatic metabolism, we generated mice with a liver-specific deletion of the *Mfn1* gene (Mfn1LKO) and monitored their energy homeostasis, mitochondrial function, and susceptibility to diet-induced insulin resistance. Livers from Mfn1LKO mice displayed a highly fragmented mitochondrial network. This was coupled to an enhanced mitochondrial respiration capacity and a preference for the use of lipids as the main energy source. Although Mfn1LKO mice are similar to control mice fed a low-fat diet, they are protected against insulin resistance induced by a high-fat diet. Importantly, Mfn1 deficiency increased complex I abundance and sensitized animals to the hypoglycemic effect of metformin. Our results suggest that targeting Mfn1 could provide novel avenues to ameliorate glucose homeostasis in obese patients and improve the effectiveness of metformin.

Mitochondria are the powerhouses of the cell, converting nutrients into usable and storable energy in the form of ATP and therefore playing a critical role in maintaining cellular and organismal energy homeostasis (1). Not surprisingly, mitochondrial dysfunction is a hallmark of multiple metabolic and age-related complications, including insulin resistance and type 2 diabetes (2). A fascinating feature of mitochondria is their ability to modulate their connectivity and architecture, from elongated to punctuated shapes, through fusion and fission processes (1,3). Mitochondrial fusion and fission cycles are believed to balance mitochondrial bioenergetics functions with the removal of damaged mitochondria (1,3). Rapid changes in mitochondrial shape take place in several cellular conditions, including cellular proliferation (3) and differentiation (4) and in response to nutrient and hormonal inputs (5–7).

Mitochondrial outer membrane fusion in mammalian cells is controlled by the mitofusin 1 and 2 (Mfn1 and Mfn2) proteins (3). Despite the high homology between Mfn1 and Mfn2, these proteins play different noncomplementary roles, as demonstrated by germline deletion of Mfn1 or Mfn2 resulting in embryonic lethality (8). Most evidence to date indicates that Mfn1 activity is mostly devoted to mediating contacts between mitochondria, whereas Mfn2 can also influence the tethering of mitochondria with other organelles, such as the endoplasmic reticulum (ER) (3,9). In line with this, mouse embryonic fibroblasts (MEFs) devoid of Mfn1 or Mfn2 failed to display the networks of long extended mitochondrial tubules that characterize wild-type (WT) MEFs (8). The

[1]Nestlé Institute of Health Sciences, Lausanne, Switzerland
[2]École Polytechnique Fédérale de Lausanne, Lausanne, Switzerland
[3]Laboratory Genetic Metabolic Diseases, Academic Medical Center, Amsterdam, the Netherlands
[4]Institute for Research in Biomedicine (IRB Barcelona), The Barcelona Institute of Science and Technology, Barcelona, Spain
[5]Departament de Bioquímica i Biologia Molecular, Facultat de Biologia, Universitat de Barcelona, Barcelona, Spain
[6]Instituto de Salud Carlos III, CIBERDEM, Madrid, Spain

Corresponding author: Carles Cantó, carlos.cantoalvarez@rd.nestle.com.

Received 18 December 2015 and accepted 5 September 2016.

This article contains Supplementary Data online at http://diabetes.diabetesjournals.org/lookup/suppl/doi:10.2337/db15-1725/-/DC1.

relevance of mitofusins in metabolic homeostasis initially came from studies demonstrating that Mfn2 expression was dramatically decreased in the skeletal muscle from obese subjects and subjects with type 2 diabetes in association with a fragmented mitochondrial network (10). Liver-specific Mfn2 deficiency in mice increases the susceptibility to develop insulin resistance even under feeding with a regular chow diet (11). This glucose intolerance was partly attributed to an increased hepatic gluconeogenesis, in line with an increased expression of gluconeogenic enzymes, including PEPCK and glucose 6-phosphatase (G6Pase), and of transcriptional regulators of gluconeogenesis, such as the peroxisome proliferator–activated receptor γ coactivator 1α (PGC-1α) (11). This, in turn, was consequent to enhanced ER stress in response to Mfn2 deletion (11).

Given the significant role of Mfn2 in the maintenance of ER homeostasis, it was not clear to what extent deficient mitochondrial fusion per se contributes to the phenotypes observed in the Mfn2-deficient model. To address this question, we created a mouse line with liver-specific deletion of Mfn1 (Mfn1LKO). The deletion of Mfn1 led to a dramatically fragmented mitochondrial network and enhanced lipid droplet size. Surprisingly, Mfn1LKO mice displayed a higher preference for lipid use as energy substrate and increased hepatic mitochondrial function. These elements granted Mfn1LKO mice protection against high-fat diet (HFD)-induced glucose intolerance and insulin resistance, despite similar body weight gain. Furthermore, HFD-fed Mfn1LKO mice were more sensitive to the hypoglycemic effect of metformin. Our findings illustrate how the deletion of Mfn1 and Mfn2 leads to very opposite effects on liver metabolism and that selectively targeting Mfn1 could provide refined ways to improve insulin resistance and type 2 diabetes.

RESEARCH DESIGN AND METHODS

All animal experiments were performed according to national Swiss and European Union ethical guidelines and approved by the local Animal Experimentation Committee under licenses VD 2570.

Animal Care

Unless otherwise specified, mice were kept in a standard temperature- and humidity-controlled environment with a 12:12-h light-dark cycle. Mice had access to nesting material and were provided with ad libitum access to water and a commercial low-fat diet (LFD) or HFD (D12450J and D12492, respectively, from Research Diets Inc.).

Animal Phenotyping

Mice were weighed and food consumption was measured each week on the same day. Body composition was determined by EchoMRI (Echo Medical Systems, Houston, TX), and VO_2, respiratory exchange ratios (RERs), food intake, and activity levels were monitored by indirect calorimetry using the Comprehensive Laboratory Animal Monitoring system (Columbus Instruments, Columbus, OH). Glucose tolerance was analyzed by measuring blood glucose after an intraperitoneal injection of 2 g/kg glucose after an overnight fast. Insulin tolerance was measured by injecting insulin (0.75 units/kg for HFD-fed mice) after a 6-h fast. Plasma insulin was determined in heparinized plasma samples using specific ELISA kits (EMD Millipore Corp.). Animals were sacrificed at 13:00 after a 6-h fast. Blood samples were collected in heparinized tubes, and plasma was isolated after centrifugation. Tissues were collected and flash frozen in liquid nitrogen.

Cell Culture and Immunohistochemistry

MEFs were cultured in DMEM (4.5 g/L glucose) supplemented with 10% FBS, Penstrep (1%), nonessential amino acids (1%), sodium pyruvate (1%), and L-glutamine (1%). For immunofluorescence assays, MEFs were fixed with 4% paraformaldehyde, and then mitochondria were visualized by staining with anti-Tom20 antibody or by overexpressing mitochondrially targeted Mito-DsRed protein. Nuclei were stained with DAPI. For the Mfn1 recovery experiment, Myc-tagged Mfn1-overexpressing plasmids were a gift from David Chan.

Mitochondrial Isolation

Mitochondria were freshly isolated from mouse livers as previously described (12). Full details can be found in the Supplementary Data.

Respirometry Studies

Respirometry studies were performed in isolated mitochondria, liver homogenates, or permeabilized extensor digitorum longus muscle fibers using high-resolution respirometry (Oroboros Oxygraph-2k; Oroboros Instruments, Innsbruck, Austria). Respirometry analyses in permeabilized muscle fibers and liver homogenates were performed as previously described (13). Full details on the buffers and methods used for respirometry analyses in isolated mitochondria can be found in the Supplementary Data.

Statistical Analyses

Statistical analyses were performed with Prism software (GraphPad). Differences between two groups were analyzed using the Student t test (two-tailed, a $P < 0.05$ was considered significant). Data are expressed as means ± SEM. Additional statistical methods can be found in the Supplementary Data.

RESULTS

Hepatic Deletion of Mfn1 Leads to a Preferential Use of Lipids as the Energy Source

Mfn1LKO mice were generated by crossing $Mfn1^{loxP/loxP}$ mice (14) backcrossed to a C57BL/6 background (control mice) with mice expressing the Cre recombinase under the albumin promoter (15). This led to a complete ablation of *Mfn1* expression in the liver (Fig. 1*A*). The deletion of Mfn1 in the liver was accompanied by a compensatory increase in Mfn2 (Fig. 1*A*) and other proteins of mitochondrial dynamics such as optic nerve atrophy 1, dynamin-1-like protein (DRP1), and mitochondrial fission factor (MFF) expression

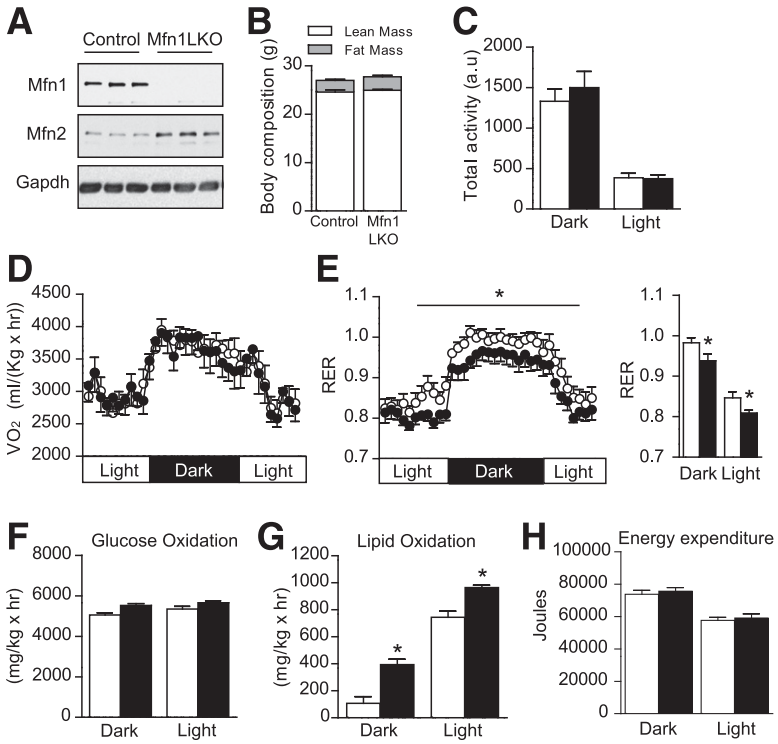

Figure 1—Hepatic deletion of Mfn1 leads to a preferential use of lipids as energy source. *A*: Mfn1and Mfn2 protein expression in the livers of control and Mfn1LKO mice. *B*: Body composition was evaluated at 12 weeks of age by EchoMRI. Total activity (*C*), total VO_2 (*D*), and RER (*E*) were measured at 12 weeks of age by indirect calorimetry. Indirect calorimetry data were used to calculate glucose oxidation (*F*), lipid oxidation (*G*), and energy expenditure (*H*). Unless otherwise stated, the white bars and circles represent control mice, and the black bars and circles represent Mfn1LKO mice. Results are shown as mean ± SEM of n = 9–10 mice per group. *$P < 0.05$, indicating statistical significance vs. the control group.

(Supplementary Fig. 1*A*), suggesting altered hepatic mitochondrial dynamics. Mfn1LKO mice had a normal appearance and were indistinguishable from the corresponding control floxed mice in body weight (Supplementary Fig. 1*B*) and composition (Fig. 1*B*). The weight of the livers from Mfn1LKO mice was similar to that of control mice (Supplementary Fig. 1*C*), as was their triglyceride content (Supplementary Fig. 1*D*). Mfn1LKO mice displayed normal food intake (Supplementary Fig. 1*E*) and daily activity (Fig. 1*C*). Indirect calorimetry analyses revealed that Mfn1LKO mice had a VO_2 similar to that of control mice (Fig. 1*D*). However, the RERs were lower in Mfn1LKO during the dark and the light phases (Fig. 1*E*), suggesting a preferential use of lipids as an oxidative energy source. This was corroborated by whole-body glucose and lipid oxidation analyses (Fig. 1*F* and *G*), which highlighted how lipid, but not glucose, oxidation was enhanced in Mfn1LKO mice, without changes in overall energy expenditure (Fig. 1*H*).

Mfn1 Ablation Leads to Higher Mitochondrial Content

The enhanced use of lipid catabolism as energy source prompted us to examine mitochondrial function in Mfn1LKO mice. Electron microscopy analyses revealed that Mfn1-deficient hepatocytes showed a higher density of mitochondria within the cytoplasm, but as expected as a result of reduced fusion rates, they had shorter maximum diameters compared with WT mitochondria (Fig. 2*A*). Hence, Mfn1 deficiency led to dramatically fragmented mitochondria. These ultrastructural measurements also indicated that despite the similar global triglyceride content, lipids were accumulated in larger lipid droplets (Supplementary Fig. 2*A*). Protein analyses in total liver homogenates reflected a specific increase in mitochondrial complex I (NADH dehydrogenase [ubiquinone] 1 alpha subcomplex subunit 9 [NDUFA9]) and complex II (succinate-ubiquinone oxidoreductase [SDHA]) content (Fig. 2*B*). These differences prompted us to directly evaluate mitochondrial function in livers from control and Mfn1LKO mice. For this purpose, we initially performed high-resolution respirometry analyses in isolated hepatic mitochondria. Although state 2 respiration, using malate and glutamate (M+G), was similar between genotypes (Fig. 2*C*), state 3 was markedly increased in mitochondria from Mfn1LKO mice (Fig. 2*C*). This was reflected in an ~23% increase in M+G respiratory control (RC; calculated as state 3–to–state 2 ratio) of Mfn1LKO hepatic mitochondria. In addition, maximal respiration, upon addition of carbonyl cyanide-4-(trifluoromethoxy)phenylhydrazone (FCCP), was also increased in the mitochondria from Mfn1LKO livers (Fig. 2*C*). When similar tests were performed for complex II, state 2 and state 3 respiration, as well as maximal respiration, were increased (Fig. 2*C*). Interestingly, RC was similar between genotypes, indicating that changes in RC

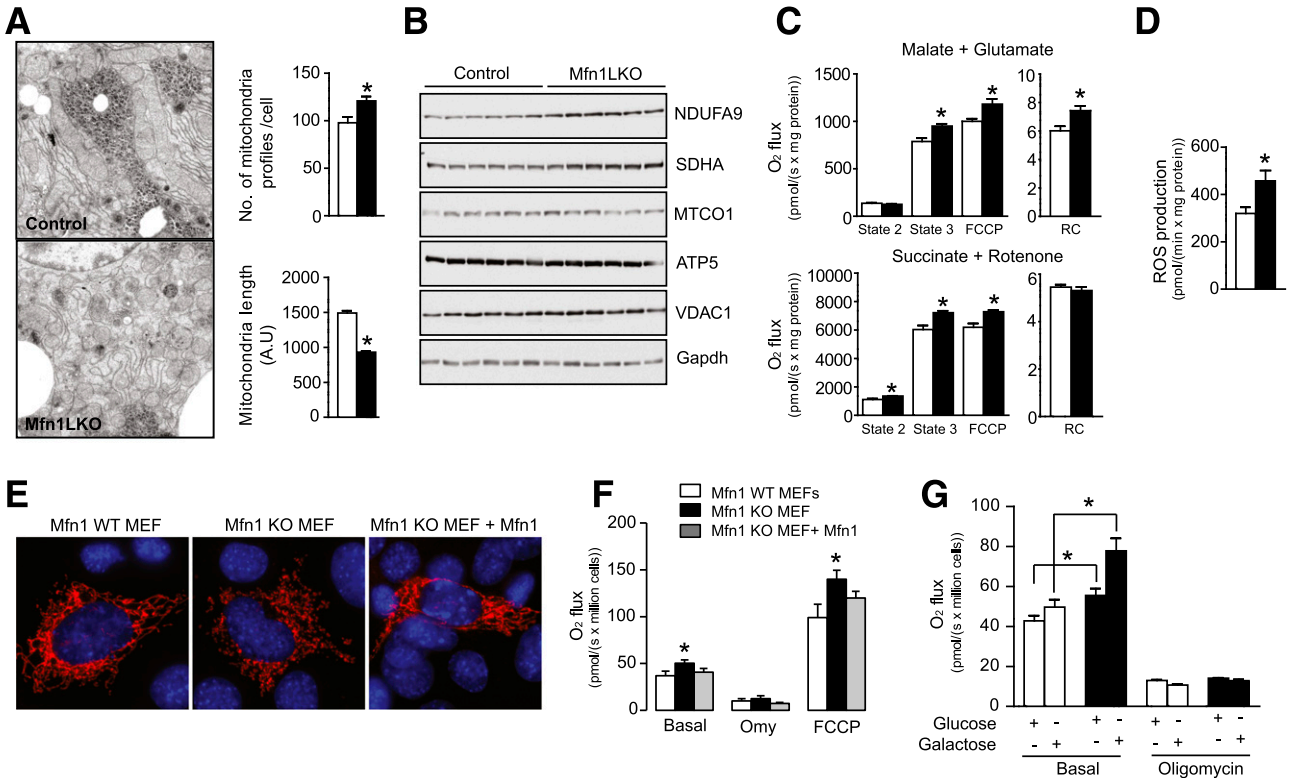

Figure 2—Mfn1 ablation leads to higher mitochondrial content. *A*: Electron microscopy of the livers from control and Mfn1LKO mice and evaluation of mean number of mitochondrial profiles and mitochondrial lengths from 20 hepatocytes from each mouse. *B*: Immunoblotting of total liver homogenates from control or Mfn1LKO mice revealed increased mitochondrial complex I (NDUFA9), complex II (SDHA), and voltage-dependent anion-selective channel protein 1 (VDAC1) protein expression. *C*: Mitochondrial respiratory capacity was analyzed in isolated mitochondria from control or Mfn1LKO mouse livers. On the top panels, state 2 respiration was measured after the addition of malate (2 mmol/L) and glutamate (10 mmol/L). ADP (250 μmol/L) was then added to measure state 3 respiration. Subsequently, FCCP was gradually titrated until maximal respiration was achieved. RC was calculated as the ratio between state 3 and state 2 respiration. On the bottom panels, similar experiments were performed, but instead of malate + glutamate, respiration was stimulated using succinate (10 mmol/L) while blocking complex I with rotenone (0.5 μmol/L). *D*: Measurement of ROS production by Amplex Red in isolated liver mitochondria from control and Mfn1LKO mice during state 2 respiration. *E*: Mitochondrial morphology in WT and Mfn1KO MEFs, transfected with mitochondrially targeted Mito-DsREd fluorescent protein and with Myc-Mfn1. *F*: Mitochondrial respiratory analyses in WT (white), Mfn1KO (black), or Mfn1KO MEFs transfected with Myc-Mfn1 (gray). After the basal respiration in media containing 25 mmol/L glucose was measured, oligomycin (Omy) (2.5 μmol/L) was added to evaluate the contribution of coupled respiration to total respiration. Then, FCCP was used to evaluate maximal respiratory capacity, before the addition of rotenone and antimycin (2.5 μmol/L) to block mitochondrial respiration. *G*: Respirometry analyses in WT and Mfn1KO MEFs in medium containing 5 mmol/L glucose or 5 mmol/L galactose. Unless otherwise stated, white bars represent control groups, and black bars represent Mfn1-deficient groups. Results are shown as mean ± SEM. *$P < 0.05$, indicating a statistically significant difference vs. the control group.

are restricted to M+G. These observations were corroborated when similar tests were done on liver homogenates instead of isolated mitochondria, where increases in state 3 respiration, but not in state 2, were observed upon stimulation with M+G (Supplementary Fig. 2*B*). This rendered an increase in RC, using M+G, of ~17% (Supplementary Fig. 2*B*). Importantly, when state 2, state 3, and RC, using M+G, were examined in permeabilized extensor digitorum longus muscle from Mfn1LKO mice, no differences were observed compared with control mice (Supplementary Fig. 2*C*), testifying that the increase in state 3 respiration was confined to the tissue where Mfn1 was ablated. Interestingly, we also observed an increase in reactive oxygen species (ROS) production in mitochondria from Mfn1LKO livers (Fig. 2*D*). To evaluate whether increased ROS production could lead to any liver damage or apoptotic response, we performed hematoxylin and eosin staining for liver anatomy and immunohistochemistry for cleaved caspase 3 as an apoptotic marker. However, no differences were found between genotypes (Supplementary Fig. 2*D*). This was further confirmed by the lack of changes in an independent readout of oxidative stress, such as the level of 4-hydroxy-2-nonenal (HNE), a marker for lipid peroxidation (Supplementary Fig. 2*E*). Therefore, the increased ROS production in Mfn1LKO mitochondria did not alter any of the markers of liver damage examined.

We next wondered whether the changes in mitochondrial content and respiration driven by Mfn1 deficiency were cell autonomous. As previously reported (8), Mfn1$^{-/-}$ MEFs displayed a completely fragmented

mitochondrial morphology (Fig. 2*E*). Basal respiration rates in Mfn1$^{-/-}$ cells in glucose-containing media were higher than in control cells (Fig. 2*F*). This was caused by higher coupled respiration, because respiration levels were similar on both genotypes after being treated with oligomycin, an inhibitor of ATP synthase. Finally, FCCP-induced maximal respiration was higher in Mfn1$^{-/-}$ MEFs (Fig. 2*F*), in line with elevated levels of complex I and overall total mitochondrial protein content (Supplementary Fig. 2*F*). To fully certify Mfn1 deletion as the cause for the respiratory changes observed in Mfn1$^{-/-}$ MEFs, we performed experiments where we reintroduced Mfn1 in Mfn1$^{-/-}$ MEFs by overexpressing a Myc-tagged Mfn1 form (Myc-Mfn1). Mfn1$^{-/-}$ MEFs transfected with Myc-Mfn1 tilted the mitochondrial dynamics toward a fusion phenotype, rendering mitochondria more filamentous (Fig. 2*E*). This was linked to a reduction in basal and maximal respiration capacity (Fig. 2*F*), indicating that Mfn1 deficiency is enough to enhance cellular-coupled respiratory capacity in a cell-autonomous fashion.

To further support the higher oxidative capacity of Mfn1$^{-/-}$ cells, we compared the ability of WT and Mfn1$^{-/-}$ MEFs to respire in the medium containing glucose or galactose (Fig. 2*G*), the latter forcing the cells to rely on oxidative metabolism to obtain net energy synthesis. Although galactose prompted an ~15% increase in respiration rates in WT cells, the respiration rates of Mfn1$^{-/-}$ MEFs rose by ~30%. As expected, oligomycin treatment revealed that these increases were caused by enhanced coupled respiration. These results further ascertain the higher coupled respiratory capacity of Mfn1-deficient cells and tissues.

Mfn1LKO Mice Are Protected Against HFD-Induced Insulin Resistance

Several observations suggested that mitochondrial dynamics could play a role in the cellular and tissular response to lipid overload or high-caloric diets. First, acute palmitate treatment caused a marked fission of the mitochondrial network in MEF cells (Fig. 3*A*) and in AML12 hepatocytes (Supplementary Fig. 3*A*). Similar observations have been previously made in β-cells (6). Second, highly fissioned mitochondria were observed in the vastus lateralis muscle from obese patients (10), suggesting that mitochondrial dynamics are shifted toward fission events upon acute or chronic lipid overload.

To understand how Mfn1 ablation might influence nutrient handling in mice upon chronic lipid overflow, we fed Mfn1LKO mice the HFD for 8 weeks. Their body weight gain during this period was undistinguishable from that of control mice (Fig. 3*B*), as was lean and fat mass distribution (Fig. 3*C*). One key detrimental effect of HFDs in mice and men is their ability to promote insulin resistance,

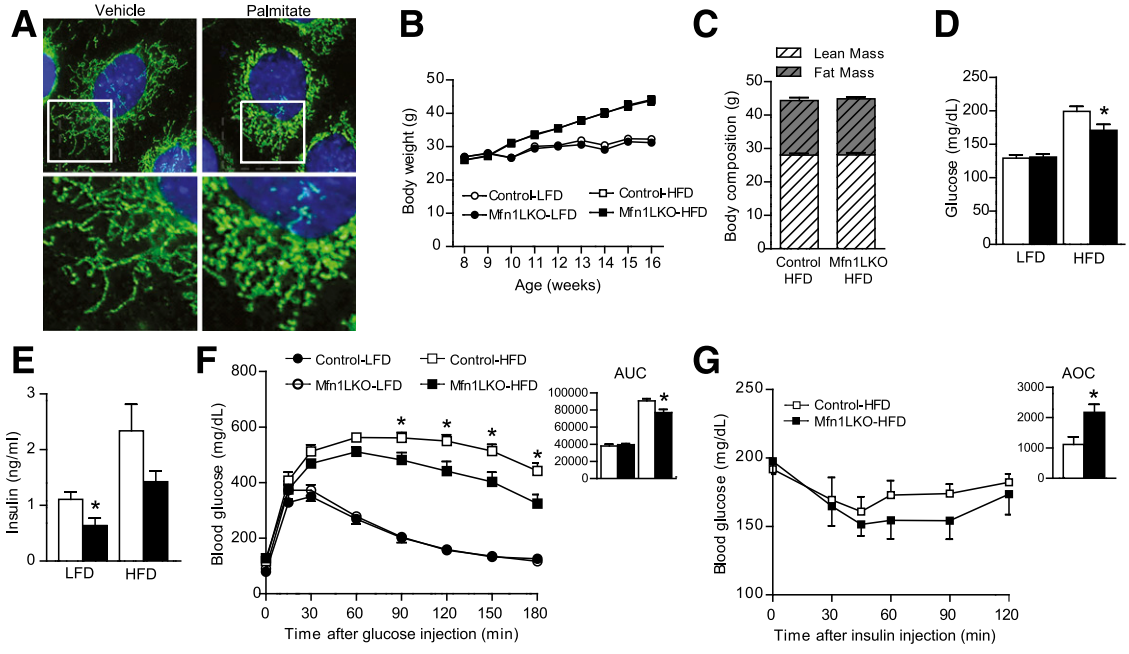

Figure 3—Mfn1LKO mice are protected against HFD-induced insulin resistance. *A*: WT MEFs were treated with vehicle or 100 μmol/L palmitate for 2 h and immunostained with antibody against Tom20 to evaluate mitochondrial architecture by immunofluorescence microscopy. *B*: Body weight evolution of control and Mfn1LKO mice fed the LFD or HFD. *C*: Body composition, measured by EchoMRI at 16 weeks of age. Circulating glucose (*D*) and insulin levels (*E*) on mice fed the LFD or HFD after a 6-h fast. *F*: Intraperitoneal glucose tolerance test was performed after an overnight fast on LFD-fed or HFD-fed control or Mfn1LKO mice. AUC, area under the curve. *G*: Insulin tolerance test was performed on control or Mfn1LKO mice fed the HFD after a 6-h fast. AOC, area over the curve. Through the figure, white is used for control mice and black is used for Mfn1LKO mice. Results are shown as mean ± SEM of n = 10 mice per group. *$P < 0.05$, indicating statistically significant difference vs. the respective control group.

ultimately leading to type 2 diabetes. Although fasting glucose levels were similar in control and Mfn1LKO mice fed an LFD, Mfn1LKO mice displayed lower fasting glycemia upon HFD treatment and a marked tendency to lower circulating insulin levels (Fig. 3*D* and *E*). This was not caused by defects in gluconeogenic gene expression (Supplementary Fig. 3*B*) and suggested higher insulin sensitivity in Mfn1LKO mice upon HFD feeding. In line with this, glucose tolerance was similar in Mfn1LKO and control mice fed the LFD, but Mfn1LKO mice were robustly protected against HFD-induced glucose intolerance (Fig. 3*F*). Similarly, insulin injections led to similar glucose excursions in control and Mfn1LKO mice under LFD conditions (data not shown), but Mfn1LKO mice retained higher insulin sensitivity after the HFD treatment (Fig. 3*G*). It has been hypothesized that insulin resistance upon HFD feeding might occur when fatty acid oxidation rates outpace the tricarboxylic acid (TCA) cycle, leading to the accumulation of acylcarnitines that may interfere with insulin sensitivity (16–18). When acylcarnitines were measured in the livers of HFD-fed Mfn1LKO mice, we observed modest reductions in most acylcarnitine species, except for C8 to C10 species (Supplementary Fig. 3*C*). Importantly, C4–3OH-carnitine has been proposed to act as a marker for insulin resistance (19), and its accumulation was considerably lower in Mfn1LKO mice (Supplementary Fig. 3*C*). Therefore, the higher TCA activity and oxidative phosphorylation rates upon HFD feeding might be better coupled in Mfn1LKO mice, preventing the accumulation of acylcarnitine species that potentially damage insulin action.

Mfn1LKO Mice Are Sensitized to the Hypoglycemic Effects of Metformin

We next performed a whole transcriptome profiling experiment with microarrays in livers from HFD-fed control and Mfn1LKO mice to unbiasedly evaluate possible mechanisms by which the latter are protected against insulin resistance. Oxidative phosphorylation and TCA cycle gene sets were the most highly upregulated in Mfn1LKO livers, according to gene set enrichment and pathway analyses (Fig. 4*A* and Supplementary Fig. 4*A*). Interestingly, these analyses also highlighted several complex I subunits as the most upregulated genes in Mfn1LKO livers (Fig. 4*A*, oxidative phosphorylation panel). In line with this, and as observed in the LFD, state 3 respiration and RC, using M+G, were largely increased in isolated mitochondria from livers of HFD-fed Mfn1 mice (Fig. 4*B*). Also in parallel with the results on the LFD, state 2, state 3, and maximal respiration were markedly increased when succinate was used as the oxidative substrate, but this did not lead to changes in the RC (Fig. 4*B*).

Complex I inhibition and the subsequent deregulation of the AMP-to-ATP ratio are considered to be key for the hypoglycemic action of metformin (20), the most widespread antidiabetic drug. Hence, we next wondered whether Mfn1 deficiency in the liver could affect metformin action. For this purpose, we performed a metformin tolerance test in HFD-fed control and Mfn1LKO mice. As expected, metformin lowered glycemia in HFD-fed control mice (Fig. 4*C*). Surprisingly, the hypoglycemic action of metformin was largely amplified in Mfn1LKO mice (Fig. 4*C*). In line with previous observations (21), metformin-triggered alterations in energy homeostasis were not sufficient to manifest into changes in AMPK activity in control livers. In contrast, the livers from metformin-treated Mfn1LKO mice displayed a high AMPK activation (Fig. 4*D*), testifying for a higher effect of metformin on the cellular energy balance. This, in turn, led to increased metformin-induced phosphorylation of nutrient-signaling proteins targeted by AMPK, such as Raptor, from the mammalian target of rapamycin complex I and cAMP response element binding protein–regulated transcription coactivator 2 (CRTC2) (Fig. 4*D*). We next evaluated whether Mfn1 deletion affected the ability of metformin to directly inhibit complex I in isolated hepatic mitochondria from HFD-fed mice. Respirometry analyses in isolated liver mitochondria revealed that metformin treatment decreased M+G state 3 respiration in a dose-dependent manner in both genotypes (Fig. 4*E* and Supplementary Fig. 4*B*). The effects, however, were more marked on Mfn1-deficient mitochondria, and state 3 respiration was comparable between control and Mfn1LKO mice at a concentration of 5 mmol/L metformin (Fig. 4*E*). Similarly, metformin dose-dependently decreased M+G RC in both control and Mfn1LKO hepatic mitochondria, albeit in a more marked fashion in the latter (Fig. 4*E*, right panel, and Supplementary Fig. 4*B*, bottom panel). In fact, metformin rendered M+G RC comparable between genotypes at 3 mmol/L concentrations (Supplementary Fig. 4*B*). Hence, these results suggest that hepatic Mfn1 deficiency sensitizes state 3 respiration and RC to metformin. Notably, metformin did not blunt the differences between genotypes in state 3 respiration when succinate was used as the oxidative substrate (Fig. 4*F* and Supplementary Fig. 4*C*), testifying for a specific effect on complex I.

DISCUSSION

In this work, we have explored how mitochondrial dynamics, and more particularly, blunted mitochondrial fusion, affect nutrient handling. Previous studies have documented an association of mitochondrial fragmentation with situations of nutrient excess, including obesity (1). Also, in certain cell types, such as primary brown adipocytes, mitochondrial fission is a physiological response favoring energy dissipation in response to a nutrient overload (5). However, recent evidence indicates that impaired hepatic mitochondrial fission might also raise energy expenditure (22). In our mouse model, Mfn1 deficiency in the liver led to enhanced lipid use and mitochondrial biogenesis. The enhanced lipid droplet size and decreased accumulation of numerous acylcarnitine species support the notion that Mfn1-deficient livers might contribute to better lipid

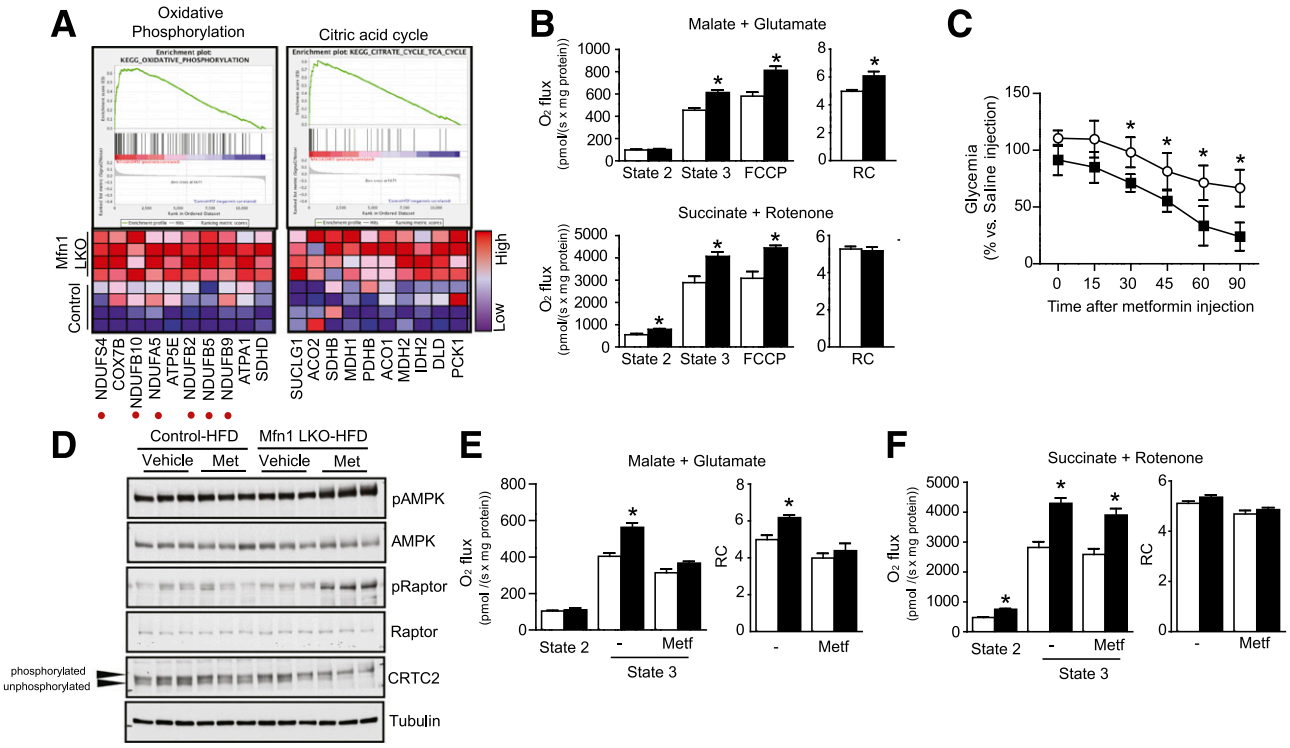

Figure 4—Mfn1LKO mice are sensitized to the hypoglycemic effects of metformin. *A*: Gene Set Enrichment Analysis was performed on the microarray data sets obtained from liver RNA from HFD-fed control or Mfn1LKO mice. Highlighted with red pearls are the enriched complex I subunits. KEGG, Kyoto Encyclopedia of Genes and Genomes. *B*: Mitochondrial respirometry analysis in isolated mitochondria from livers of control and Mfn1LKO mice fed the HFD were performed as described for Fig. 2*C*. *C*: Mice were intraperitoneally injected with 250 mg/kg metformin or saline for 3 consecutive days at 8:00 A.M. We performed a metformin tolerance test on mice fasted overnight by injecting 250 mg/kg metformin or saline, and blood glucose was measured at the indicated times. *D*: The HFD-fed control or Mfn1LKO livers were flash frozen after the metformin tolerance test, homogenized, and immunoblotted for phosphorylation (p) of AMPK and its downstream targets Raptor and CRTC2 to evaluate the effect of metformin-mediated hepatic signaling. *E*: Mitochondria were isolated from control and Mfn1LKO livers. Then, state 2 and state 3 respiration were analyzed by adding M+G in the presence or absence of ADP (5 mmol/L). Then, metformin was sequentially added at increasing concentrations after the assessment of state 3 respiration. Mitochondria were incubated for 10 min after each step (see Supplementary Fig. 4 for the whole panel). Total respiration values, with and without metformin treatment, are shown on the left. Changes in the RC induced by metformin are shown on the right. *F*: As in *E*, but succinate was used as the oxidative substrate, together with rotenone to inhibit complex I respiration. Through the figure, white bars and circles depict the control group, and black bars and circles are used for the Mfn1LKO group. Results are shown as mean ± SEM of n = 4–10 mice per group. *$P < 0.05$, indicating statistically significant differences vs. the control group.

handling and coupling to fatty acid oxidation. This, in turn, could help prevent the accumulation of secondary lipid species that could interfere with insulin action and the generation of multilocular lipid droplets, which are characteristic of hepatic mitochondrial dysfunction and steatohepatitis (23). Therefore, our work supports the idea that mitochondrial fragmentation occurring in HFD-fed mice and obese patients (10,24) may not be deleterious per se and might actually be an adaptive mechanism to cope with fat overflow.

It is important to note, however, that we have only investigated the effect of mitochondrial fission triggered by Mfn1 deficiency, which might not be generalized to all kinds of mitochondrial fission events. Mitochondrial fission can also be controlled physiologically by Mfn1-independent mechanisms such as reductions in Mfn2 or increases in Drp1 activity (3). A recent report linked hepatic mitochondrial fragmentation with metabolic disease, based on a model with impaired Mfn2 activity (11). However, Mfn2 not only mediates intermitochondrial contact but also participates in the communication of mitochondria with other organelles such as the ER (9,25). Consistently, defective Mfn2 expression in the liver triggers ER stress, driving whole-body insulin resistance (11). In contrast, deletion of Mfn1 in the liver did not cause ER stress (Supplementary Fig. 5*A* and *B*). Because Mfn1 and Mfn2 are both controlled by similar transcription factors, such as PGC-1α and estrogen-related receptor-α (ERR-α) (26), disentangling their expression physiologically might be difficult. Hence, only limited reductions in the Mfn1 gene might be physiologically possible in situations of nutrient excess without dragging the organism into the metabolic imbalances caused by the subsequent reduction in Mfn2 expression. Nonetheless, our results show that genetic and pharmacological strategies aimed to specifically reduce Mfn1 activity could be helpful in the management of glucose homeostasis in situations of insulin resistance and type 2

diabetes. In this sense, it is important to note that Mfn1 activity is not exclusively controlled through transcriptional means but also by posttranslational mechanisms. For example, Mfn1 activity can be inhibited via acetylation of K222, which blunts Mfn1 GTPase activity (27). Similarly, Mfn1 can be phosphorylated at T562 by the extracellular-regulated kinase path, an event that compromises Mfn1 oligomerization and function (28). Interestingly, higher mitochondrial protein acetylation levels (29) and higher extracellular-regulated kinase signaling (30) have been observed in models of obesity, in line with a downregulation of Mfn1 activity and enhanced mitochondrial fragmentation.

In contrast to a decrease in mitochondrial respiration in Mfn2LKO livers (11), Mfn1 deletion in hepatocytes led to a marked increase in state 3 and maximal respiration, driven by M+G or succinate. In the cases of M+G, a higher RC was observed in isolated hepatic mitochondria and liver homogenates from Mfn1LKO mice. A higher state 3 respiration with succinate + rotenone and a higher RC with M+G have also been observed in Mfn1-deficient cardiomyocytes (31). Altogether, these data suggest that Mfn1 deficiency prompts a higher capacity for substrate oxidation and ATP turnover. Our results highlight an increase in the activity of complex I–IV, as well as complex II–IV, which are in line with the increases in complex I and complex II subunits protein levels. Because changes in complex III and IV protein levels were not observed, these results suggest that complex III and complex IV are not limiting for complex I–IV or complex II–IV activities in livers from control mice. Alternatively, our studies cannot rule out a potential intrinsic activation of complex III and IV in Mfn1LKO mitochondria.

The definite reasons why Mfn1 deletion affects mitochondrial content and qualitative respiration are unclear, but could rely on mitohormetic and/or proteostatic responses. First, Mfn1 deficiency led to higher ROS production. This is in line with the higher complex I activity in Mfn1-deficient cells, because complex I is one of the main contributors to superoxide production by mitochondria (32). Although ROS overproduction can constitute a physiological disadvantage (32), no major signs of apoptotic or oxidative damage markers were observed in the livers of Mfn1LKO mice, although more subtle effects cannot be ruled out. Paradoxically, it has been shown that Mfn1 deficiency in myocytes can protect from ROS-induced cell death (31). Therefore, mitohormetic adaptations in response to a higher ROS production (33) might protect Mfn1-deficient mitochondria against ROS damage. On a second level, a recent study suggested that mito-nuclear protein imbalances can lead to proteostatic responses safeguarding and optimizing mitochondrial function (34). In this sense, an increase in the ratio of nuclear DNA-encoded complex II subunit SDHA to mitochondrial DNA-encoded complex IV subunit cytochrome c oxidase I was noticed in Mfn1-deficient livers (Fig. 2*B* and Supplementary Fig. 5*C*). All of these aspects will definitely merit future research.

One interesting aspect in Mfn1LKO livers is an increase in complex I activity and expression. Knowing that metformin probably exerts its therapeutic effects by altering mitochondrial respiration through complex I (35), we hypothesized that Mfn1 deficiency might affect the action of metformin. Metformin hypoglycemic action was enhanced in Mfn1LKO mice. This was mirrored by a dramatic decrease in state 3 respiration and RC using M+G at metformin concentrations in the low millimolar range. This is in agreement with recent observations in skeletal muscle mitochondria, indicating that metformin showed its most dramatic effects on state 3 respiration driven, in that case, by malate + pyruvate (36). Hence, metformin might promote a higher energy imbalance in Mfn1-deficient mitochondria. Accordingly, Mfn1 deletion exacerbated metformin-induced hepatic AMPK activation and glucose-lowering actions. Further research will be required to elucidate how Mfn1 or mitochondrial fission impinges on complex I function. One interesting possibility might rely on the interaction of Mfn1 and Mfn2 with optic nerve atrophy 1 (37), which at the same time controls cristae shape, supercomplexes assembly, and respiratory efficiency (38). Changes in the stoichiometry of these interactions might affect respiratory coupling. In this sense, RC was increased in Mfn1LKO hepatic mitochondria only upon malate-glutamate stimulation, but not with succinate, which could be related to the ability of complex I, but not complex II, to modulate its assembly with complex III and IV to form respiratory supercomplexes (39).

As a whole, this work unravels an unsuspected role of Mfn1 enhancing mitochondrial respiratory capacity and protecting against insulin resistance in situations of HFD. This, in turn, suggests that mitochondrial fission in obese patients is an adaptation to better handle lipid overflow. Finally, our results also suggest that reductions in Mfn1 levels could provide a new strategy to improve metformin-mediated effects in metformin-resistant populations.

Acknowledgments. The authors thank the members of the Cantó laboratory for exciting discussions and the members of the École Polytechnique Fédérale de Lausanne animal house for technical support.

Funding. Work in the Houtkooper group is financially supported by the European Research Council (Starting Grant No. 638290) and a ZonMw VENI grant (no. 91613050). A.W.G. is supported by an Academisch Medisch Centrum PhD Scholarship. A.Z. is supported by research grants from the Secretaría de Estado de Investigación, Desarrollo e Innovación (SAF2013-40987R), from the Agència de Gestió d'Ajuts Universitaris i de Recerca "Generalitat de Catalunya" (Grant 2014SGR48), CIBERDEM ("Instituto de Salud Carlos III"), and Instituto de Salud Carlos III (PIE14/00045). A.Z. is a recipient of an ICREA "Academia" (Generalitat de Catalunya).

Duality of Interest. S.S.K., M.J., M.B., J.R., F.R., S.M., P.D., and C.C. are employees of Nestlé Institute of Health Sciences S.A. No other potential conflicts of interest relevant to this article were reported.

Author Contributions. S.S.K., M.J., M.B., J.R., A.W.G., C.M., M.I.H.-A., F.R., and S.M. performed the experiments. S.S.K., F.R., P.D., R.H.H., A.Z., and C.C. analyzed the data. S.S.K., A.Z., and C.C. conceived the study. S.S.K. and C.C. wrote the manuscript. All authors contributed to editing the manuscript. C.C.

is the guarantor of this work and, as such, had full access to all the data in the study and takes responsibility for the integrity of the data and the accuracy of the data analysis.

References

1. Liesa M, Shirihai OS. Mitochondrial dynamics in the regulation of nutrient utilization and energy expenditure. Cell Metab 2013;17:491–506
2. Andreux PA, Houtkooper RH, Auwerx J. Pharmacological approaches to restore mitochondrial function. Nat Rev Drug Discov 2013;12:465–483
3. Liesa M, Palacín M, Zorzano A. Mitochondrial dynamics in mammalian health and disease. Physiol Rev 2009;89:799–845
4. Kasahara A, Cipolat S, Chen Y, Dorn GW 2nd, Scorrano L. Mitochondrial fusion directs cardiomyocyte differentiation via calcineurin and Notch signaling. Science 2013;342:734–737
5. Wikstrom JD, Mahdaviani K, Liesa M, et al. Hormone-induced mitochondrial fission is utilized by brown adipocytes as an amplification pathway for energy expenditure. EMBO J 2014;33:418–436
6. Molina AJ, Wikstrom JD, Stiles L, et al. Mitochondrial networking protects beta-cells from nutrient-induced apoptosis. Diabetes 2009;58:2303–2315
7. Gao AW, Cantó C, Houtkooper RH. Mitochondrial response to nutrient availability and its role in metabolic disease. EMBO Mol Med 2014;6:580–589
8. Chen H, Detmer SA, Ewald AJ, Griffin EE, Fraser SE, Chan DC. Mitofusins Mfn1 and Mfn2 coordinately regulate mitochondrial fusion and are essential for embryonic development. J Cell Biol 2003;160:189–200
9. de Brito OM, Scorrano L. Mitofusin 2 tethers endoplasmic reticulum to mitochondria. Nature 2008;456:605–610
10. Bach D, Pich S, Soriano FX, et al. Mitofusin-2 determines mitochondrial network architecture and mitochondrial metabolism. A novel regulatory mechanism altered in obesity. J Biol Chem 2003;278:17190–17197
11. Sebastián D, Hernández-Alvarez MI, Segalés J, et al. Mitofusin 2 (Mfn2) links mitochondrial and endoplasmic reticulum function with insulin signaling and is essential for normal glucose homeostasis. Proc Natl Acad Sci U S A 2012;109:5523–5528
12. Frezza C, Cipolat S, Scorrano L. Organelle isolation: functional mitochondria from mouse liver, muscle and cultured fibroblasts. Nat Protoc 2007;2:287–295
13. Cantó C, Garcia-Roves PM. High-resolution respirometry for mitochondrial characterization of ex vivo mouse tissues. Curr Protoc Mouse Biol 2015;5:135–153
14. Chen H, McCaffery JM, Chan DC. Mitochondrial fusion protects against neurodegeneration in the cerebellum. Cell 2007;130:548–562
15. Postic C, Shiota M, Niswender KD, et al. Dual roles for glucokinase in glucose homeostasis as determined by liver and pancreatic beta cell-specific gene knock-outs using Cre recombinase. J Biol Chem 1999;274:305–315
16. Muoio DM, Neufer PD. Lipid-induced mitochondrial stress and insulin action in muscle. Cell Metab 2012;15:595–605
17. Koves TR, Ussher JR, Noland RC, et al. Mitochondrial overload and incomplete fatty acid oxidation contribute to skeletal muscle insulin resistance. Cell Metab 2008;7:45–56
18. Schooneman MG, Vaz FM, Houten SM, Soeters MR. Acylcarnitines: reflecting or inflicting insulin resistance? Diabetes 2013;62:1–8
19. An J, Muoio DM, Shiota M, et al. Hepatic expression of malonyl-CoA decarboxylase reverses muscle, liver and whole-animal insulin resistance. Nat Med 2004;10:268–274
20. Viollet B, Guigas B, Sanz Garcia N, Leclerc J, Foretz M, Andreelli F. Cellular and molecular mechanisms of metformin: an overview. Clin Sci (Lond) 2012;122:253–270
21. Madiraju AK, Erion DM, Rahimi Y, et al. Metformin suppresses gluconeogenesis by inhibiting mitochondrial glycerophosphate dehydrogenase. Nature 2014;510:542–546
22. Wang L, Ishihara T, Ibayashi Y, et al. Disruption of mitochondrial fission in the liver protects mice from diet-induced obesity and metabolic deterioration. Diabetologia 2015;58:2371–2380
23. Fromenty B, Berson A, Pessayre D. Microvesicular steatosis and steatohepatitis: role of mitochondrial dysfunction and lipid peroxidation. J Hepatol 1997;26(Suppl. 1):13–22
24. Jheng HF, Tsai PJ, Guo SM, et al. Mitochondrial fission contributes to mitochondrial dysfunction and insulin resistance in skeletal muscle. Mol Cell Biol 2012;32:309–319
25. Filadi R, Greotti E, Turacchio G, Luini A, Pozzan T, Pizzo P. Mitofusin 2 ablation increases endoplasmic reticulum-mitochondria coupling. Proc Natl Acad Sci U S A 2015;112:E2174–E2181
26. Soriano FX, Liesa M, Bach D, Chan DC, Palacín M, Zorzano A. Evidence for a mitochondrial regulatory pathway defined by peroxisome proliferator-activated receptor-gamma coactivator-1 alpha, estrogen-related receptor-alpha, and mitofusin 2. Diabetes 2006;55:1783–1791
27. Lee JY, Kapur M, Li M, et al. MFN1 deacetylation activates adaptive mitochondrial fusion and protects metabolically challenged mitochondria. J Cell Sci 2014;127:4954–4963
28. Pyakurel A, Savoia C, Hess D, Scorrano L. Extracellular regulated kinase phosphorylates mitofusin 1 to control mitochondrial morphology and apoptosis. Mol Cell 2015;58:244–254
29. Hirschey MD, Shimazu T, Jing E, et al. SIRT3 deficiency and mitochondrial protein hyperacetylation accelerate the development of the metabolic syndrome. Mol Cell 2011;44:177–190
30. Jiao P, Feng B, Li Y, He Q, Xu H. Hepatic ERK activity plays a role in energy metabolism. Mol Cell Endocrinol 2013;375:157–166
31. Papanicolaou KN, Ngoh GA, Dabkowski ER, et al. Cardiomyocyte deletion of mitofusin-1 leads to mitochondrial fragmentation and improves tolerance to ROS-induced mitochondrial dysfunction and cell death. Am J Physiol Heart Circ Physiol 2012;302:H167–H179
32. Brand MD, Affourtit C, Esteves TC, et al. Mitochondrial superoxide: production, biological effects, and activation of uncoupling proteins. Free Radic Biol Med 2004;37:755–767
33. Ristow M, Schmeisser S. Extending life span by increasing oxidative stress. Free Radic Biol Med 2011;51:327–336
34. Houtkooper RH, Mouchiroud L, Ryu D, et al. Mitonuclear protein imbalance as a conserved longevity mechanism. Nature 2013;497:451–457
35. Foretz M, Guigas B, Bertrand L, Pollak M, Viollet B. Metformin: from mechanisms of action to therapies. Cell Metab 2014;20:953–966
36. Andrzejewski S, Gravel SP, Pollak M, St-Pierre J. Metformin directly acts on mitochondria to alter cellular bioenergetics. Cancer Metab 2014;2:12
37. Guillery O, Malka F, Landes T, et al. Metalloprotease-mediated OPA1 processing is modulated by the mitochondrial membrane potential. Biol Cell 2008;100:315–325
38. Cogliati S, Frezza C, Soriano ME, et al. Mitochondrial cristae shape determines respiratory chain supercomplexes assembly and respiratory efficiency. Cell 2013;155:160–171
39. Lapuente-Brun E, Moreno-Loshuertos R, Acín-Pérez R, et al. Supercomplex assembly determines electron flux in the mitochondrial electron transport chain. Science 2013;340:1567–1570